Al Azhar Bulletin of Science Vol. 27, No. 2 (December) 2016, pp. 65-72

GEOMORPHOLOGY AND MINERALOGY OF THE TOP METER BLACK SANDS NORTH WEST OF EL-BURBLLUS LAKE, KAFR AL-SHEIKH GOVERNORATE, EGYPT.

El-Afandy, A. H. , Moustafa, M.I., El Nahas, H.A., Abdou, A. A. and Barakat, M. G.

Nuclear Material Authority, P.O. Box 530 Maadi, Cairo, Egypt.

ABSTRACT

*Geomorphologically, the study area comprises three geomorphic units, the foreshore zone, the backshore flat and coastal sebkhas. El-Sahel (coastal) drain runs parallel to the shoreline. The coastal plain of study area is divided to northern and southern sectors; each sector covers an area of about 10Km**2**. The northern sector is characterized by relatively highly concentrated black sand especially the near shore area due to marine erosion and the southern sector is characterized by diluted homogenous sediments compared with the northern one.*

Along the shoreline of the study area, erosion and accretion phenomena are indicated by alternations of highly concentrated and low concentrated sediments, distribution of flaky, discoidal, spherical stones and mud balls. The north-western part of the northern coastal plain sector of the study area is characterized by the highly concentrated black sands extends from the fifth groin eastward about 2.5 Km. These deposits are affected greatly by a wave cut along the shore line. Rate of shoreline retreat along Abu-Khashabah beach in front of El-Matlaa Medak (road) was 43.66 m/y in the time interval between 2003 and 2012.

The coastal plain of study area was covered by a total 561 collected samples at one meter depth from the surface were collected within a grid pattern 200m×200m nearly parallel and perpendicular to the shoreline. The northern sector of coastal plain area is covered by 255 samples, whereas the southern sector covered by 306 samples. Naturally highly concentrated black sands are deposited in a thin mantle near and parallel to the shoreline of the northern coastal plain sector. The highly concentrated black sands were scraped from the mantle to a depth of about 30 cm.

Separation of economic heavy minerals Concentrates using physical ore dressing technique is considered closer to reality; cheap and safe method than the heavy fluid technique.

The average content (Av. cont.) and reserve tonnage for each economic mineral in the studied sectors are: magnetite has an average content 11.61% with a reserve 296055 ton, ilmenite has an average content 33.74% with a reserve 860370 ton, garnet has an average content 2.88% with a reserve 73440 ton, leucoxene has an average content 2.58% with a reserve 65790 ton, zircon has an average content 4.11% with a reserve 104805 ton, rutile has an average content 1.26% with a reserve 3210 ton and monazite has an average content 0.05% with a reserve 1275 ton with a total average of economic minerals 56.23% and reserve of 1433865 tons.

INTRODUCTION

The Egyptian black sands occur along the northern coastal plain from Abu Qir in the west to Rafah in the east. They are well represented in four localities namely, the beach area of Rosetta, Damietta, north Sinai and the coastal sand dunes of El-Burullus-Baltim area. The northern coastal plain of the Nile Delta and Sinai varies in width from several meters to several kilometers; also, exploratory drilling showed that these deposits extend downward at some places to a depth of more than 20m. Actually, the black sand deposits are considered as one of the most important mineral resources in Egypt.

The main part of the Egyptian beach minerals comes from volcanic, igneous and metamorphic rocks of the upper reaches of the Nile River and its main tributaries as, Blue Nile (60%) & Atbara River (26%), (Ethiopian highland) and White Nile (14%), (Equatorial plateau), Wassef (1964). The greatest part of black sands accumulated in Rosetta area.

The grade and reserve of the economic heavy minerals of the Egyptian black sands are appreciably high compared tp other similar major world occurrences (Hammoud, 1966). Since the early sixtieth and up till now, the Egyptian black sands were subjected to extensive evaluation approaches by different authorities and organizations as, [EBASCO (1964), El-Shazly (1965), Dabbour (1973,1980), Hammoud (1985), Robertson Research International (RRI) limited company

(1985), Dabbour (1994), El-Hadary (1998), Abdel-Fattah (2008), and El-Shafey (2011)]. The Nuclear Materials Authority (NMA) constructed a semi-industrial plant for the exploitation of the black sands at Rosetta Town and Abu-Khashabah Village th the east of Rosetta. For the completion and continuation of this plant to extract the economic heavy minerals on industrial scale, near and accessible area of high potentiality free from human activity is required for further expansion of this production line. Consequently, geomorphology and mineralogy of the top meter black sands north west of El-Burullus Lake, Kafr Al-Sheikh Governorate, Egypt are the main goals of the present study

Location and geomorphology of the study area.

The study area lies on the Mediterranean Sea Coast, about 8Km east of Rosetta distributary mouth, north-west of El- Burullus lake between Longitudes 30˚ 25' 48" - 30˚ 33' 00" E and Latitudes 31˚ 26' 42" - 31˚ 27' 18" N. It covers an area of about 20Km**2**, with 10Km long parallel to the shoreline and two kilometers width nearly perpendicular to the shoreline, (Fig. 1).

The beach area in the front of seawalls was completely eroded and the sea water in direct contact with the seawall, (Fig. 2B). Moreover the sea water begins to pull the sands under/between the root of the eastern seawall, this indicated by the distribution of caves behind the seawall, (Fig. 2D). The down drift side of the eastern seawall is affected greatly by erosion and retreat of the shoreline, so, about 200m small seawall parallel to the shoreline was constructed on the south-eastern side of the main seawall, but the sea water drop in Birkat Ash-Shuqaqi which situated just south of the main seawall from the unprotected areas along the shoreline, (Fig. 2E).

The rate of shoreline changes after protection reveals that the two seawalls have succeeded in stopping the shoreline erosion along the tip of Rosetta promontory. However, they shifted the erosion to down drift side of the seawalls, (Fig. 2C). Two sets of groins were constructed since 2003 to minimize the shore erosion and stabilize the eastern and western banks of the promontory. These groins are built perpendicular to the shoreline to trap moving sand and widen the beach. The lengths of these groins vary between 400 and 500 meters and spaced 800 to 900 meters apart. The recently highly concentrated black sands formed along the beach face east of the fifth groin to about 500m east of the guard station number 63; indicate the changing of the western part of Abu-Khashabah beach from zone of accretion to zone of erosion, (Fig. 3). Rate of shoreline retreat along Abu-Khashabah beach in front of El-Matlaa Medak was 43.66 m/y in the time interval between 2003 and 2012. To retreat erosion process along Abu-Khashabah beach, four groins must be added eastward from the last groin to reach to the widest coastal plain

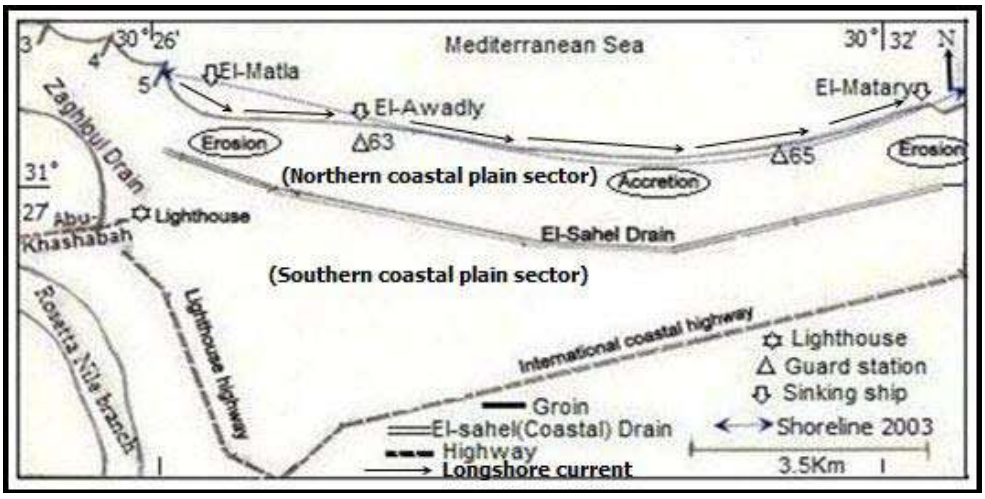

Figure 1: Location and accessibility of the study area.

area, far from the river bend at Abu-Khashabah Village. Generally, the months, July, August and September are recommended for constructing the protective engineering structures. Fortunately, eastward from the guard station number 65, the coastline trend (NE-SW) is perpendicular to the direction of waves action, the reason reduces greatly the rate of erosion.

Abu-Khashabah beach face is mostly smooth with a gentle slope (2˚ -5˚) except the western sector which is characterized by slightly steeper slope. The effect of the gentle slope is to absorb nearly all the energy approaching from offshore, so there are no strong waves acting on the beach except when abnormal stormy conditions are present. A few sand dunes and sand hillocks (< 2m in elevation) are distributed along the coastal plain area .These dunes tend to begin developed as a wind shadow deposits in the lee of vegetation or other obstruction. Sand hillocks are embryonic dunes with heights ranging between a few centimeters and a few meters. They have domal shapes; their windward sides are covered

Figure. 2: Erosion process around the eastern sea wall of Rosetta promontory.

Figure. 3: Photograph showing Abu-Khashabah beach and highly concentrated black sand distributed along the shoreline as well as wave cut due to marine erosion.

by some herbs and shrubs that help in the fixation of hillocks.

In winter season, with drop out of fresh water, the south-eastern sector of the study area is characterized by flourishing of bushes, reeds, and grasses in slightly elevated areas with death and disintegration of these plants in summer season, the organic matter increased annually in the top meter of the beach sediments. Also in winter season and during stormy condition the sea water carried clay and dissolved materials as a result of marine erosion of clay lenses of the continental shelf covered the low areas of Abu-Khashabah coastal plain especially the study area until the International coastal highway.

In summer season the southern coastal plain of the study area is characterized by the distribution of seepage of clay and organic matter in some low elevated areas. Also, in summer season, with evaporation and the formation of salt crusts, some pockets of study area was utilized in non domestic salt production.

Parallel and cross lamination are shown by digging number of trenches in the coastal plain area of the northern and southern sectors. During reconnaissance field works it was observed that, sea crabs are usually dig up holes in the beach sand, the colour of the excavated sand indicates the presence or absence of highly concentrated sediments in the subsurface.

Along the shoreline of the study area, erosion and accretion phenomena are indicated by the presence of alternation of high and low concentrated sediments, distribution of flaky, discoidal, spherical stones and mud balls. The flaky marl stone fragments and mud balls were derived from submarine banks of the present and old Nile branches (Frihy et al., 1988). Discoidal and spherical stones were formed due to reworking of rock fragments under the effect of waves action in a high energy environment, El-Fishawi and Molnar (1981), El-Fishawi (1984).

The north-western part of the northern is characterized by highly concentrated black sands which extend from the fifth groin eastward about 2.5 Km. These deposits are affected greatly by a wave cut along the shore line (Fig. 4). On the other hand, the north-eastern sector of the study area is characterized by relatively diluted heavy minerals black sand, gentle slope beach face and cusps structures were observed along the shoreline, (Fig. 4B).

Sampling of the study area.

The coastal plain of the study area is nearly rectangular in shape, 10Km long parallel to the shoreline and 2Km width nearly perpendicular to the shoreline. El-Sahel (coastal) drain which runs parallel to the shoreline divides the coastal plain area into northern and southern sectors. The northern sector is bounded from the north by the Mediterranean Sea and from south by El-Sahel drain. It is characterized by relatively highly concentrated black sand especially in the near shore area. The southern sector is bounded from the north by El-Sahel drain and from the south by the international highway and characterized by diluted homogenous sediments compared with the northern sector.

From the field visual observation, the northern coastal plain sector of the study area is more concentrated in heavy minerals characterized by the darker color compared to the southern sector. On the other hand, the southern sector of coastal plain area is characterized by a light tone in colour, rich in clay and organic matter. The coastal plain area was covered by 561. samples to a depth of one meter at the intersection of a grid pattern 200m×200m nearly parallel and perpendicular to the shoreline. The northern sector of coastal plain area is covered by 255 samples whereas the southern sector is covered by 306 samples, (Fig.5).

The collected samples in the northern sector of coastal plain area are distributed along five profiles parallel to the shoreline. The southern sector of coastal plain area distributed along six profiles parallel to the shoreline. Every profile comprises 51 samples taken the symbol of the profile and numbered from 1 to 51 from west to east. The distance between the northern profile and the shoreline varies

Figure 4: Photographs showing wave cut (A) and cusps structures (B) along the shoreline of the study area.*El-Afandy et al., Geomorphology and Mineralogy*

Figure 5: Satellite map showing location of field samples.

between 50m and 100m and that between the southern profile and the international coastal road ranges from 2Km in the west to 200m in the east. Naturally highly concentrated black sands are deposited in a thin mantle near and parallel to the shoreline of the northern coastal plain sector. The thickness of the mantle ranging from 10 cm to 40 cm with an average about 30cm and the width is variable, ranging from few meters up to 40 meters with an average about 20 meters. It extends about 2.5 km along the shoreline from Medak El-Matlaa eastward till the east of the guard station number 63. The highly concentrated black sands were scraped from the mantle to a depth of about 30 cm. The collected sands were stored in an open store at Abu-Khashabah site where a processing pilot plant was constructed.

A representative sample prepared from the collected samples subjected to separation of heavy economic minerals using physical ore dressing technique.

Concentration of economic heavy minerals using physical ore dressing technique.

All distributed along 51 profiles nearly perpendicular to the shoreline. Each profile composed of six samples in the southern sector and five samples from the northern sector, from which one representative sample was prepared by mixing one quarter of each sample together. So, the southern and northern coastal plain sectors were covered by 51 composite samples from each sector. Each composed representative sample was subjected to heavy minerals concentration using Wilfley shaking table to obtain first heavy mineral concentrate (H1.C). Each first heavy mineral concentrate (H1.C) was repeated again to obtain economic heavy mineral concentrate (H2.C). The average percentage of first heavy mineral concentrate (H1.C) and the economic heavy mineral concentrate (H2.C) are 5.76% and 3.84% for the southern sector and 6.43% and 4.77% for the northern sector.

Each economic heavy mineral concentrate (H2.C) of the Wilfley shaking table was subjected to magnetic separation using Low intensity wet drum Magnetic separator for big and highly concentrated samples or by using Frantz, Ferro-filter Magnetic separator for small and diluted samples. The separated magnetite was weighed and its percentage relative to the weight of the original sample has an average 1.18% for the southern sector and 1.63% for the northern one.

A representative composite sample was prepared from the magnetite free economic heavy fractions. The prepared sample was subjected to magnetic fractionation using the Frantz Isodynamic Separator modal, (L-1). The selected separation electric currents are 0.2, 0.5, 1.0 and 1.5 ampere respectively. The chosen settings for magnetic fractionation were, side slope 5˚, forward slope 20˚ and the feeding rate should be very low in order to give complete chance for each particle to move in the appropriate magnetic path. So, five magnetic sub-fractions were obtained which are the magnetic sub-fraction at 0.2 ampere, the magnetic sub-fraction at 0.5 ampere, the magnetic sub-fraction at 1.0 ampere, the magnetic sub-fraction at 1.5 ampere and the non-magnetic sub-fraction at 1.5 ampere, the percentage of each magnetic sub- fraction were calculated and quoted in Table (1).

Microscopic investigation.

Each free magnetite sub-fraction was subjected to microscopic examination using binocular stereomicroscope and transmitted polarizing light microscope. About 1000 mineral particles were identified and counted, from different microscopic field covering the entire prepared slide. The frequency of each recorded mineral in the slide was calculated by multiplying the number of its particles by both its specific gravity and by one hundred. The product was divided by the sum of the products of the multiplication of the number of each present mineral particle by its specific gravity. The weight of each mineral in the different magnetic sub-fraction was calculated and summed to represent the total mineral weight in the sample. The frequency of each mineral in the original sample was calculated and the results were tabulated in Table (2).

Table 1: Magnetic fractionation of economic heavy minerals obtained by ore dressing techniques along the southern coastal plain sector.

	Magnetite	Mag. 0.2A	Mag. 0.5A	Mag. 1.0A	Mag. 1.5A	N.Mag. 1.5A
	(Wt. %)	(Wt. %)	(Wt. %)	(Wt. %)	(Wt. %)	(Wt. %)
S. Sector	1.18	2.057	0.399	0.027	0.018	0.155
N.Sector	1.63	2.42	0.48	0.04	0.03	0.17

Table 2: Frequency of the heavy economic minerals obtained by ore dressing techniques.

	T.E.M. %	Magt. %	Ilm. %	Gar. %	Leu. %	Zir. %	Rut. %	Mon. %
S. Sector	3.47	1.13	1.96	0.13	0.08	0.12	0.040	0.0055
N. Sector	4.71	1.63	2.53	0.19	0.12	0.17	0.06	0.01

The highly concentrated black sands were scraped from the mantle to a depth of about 30 cm. A representative sample was prepared from the collected sands and subjected to ore dressing technique for concentration and separation of heavy economic minerals using a simple flowsheet showing in Fig. (6). The prepared sample was subjected firstly to sun dry and screened using a 2mm screen to remove coarse waste and shell fragments. The flowsheet was suggested to beneficiate the main and trace economic minerals by the using of gravitational, magnetic, and electrostatic methods. The frequencies of economic minerals in the highly concentrated black sands are shown in (Table 3).

Estimation of the raw sand tonnage.

The study coastal plain sectors characterized by low relief which are more or less plained surface so that the volume of sand of each sector is roughly calculated as length x width x depth in m3. The tonnage of the raw sand was calculated by multiplying the volume by the calculated average apparent density of the raw sand, (Table 4).

Estimation of the total economic mineral reserves:-

The tonnage of total economic minerals was calculated by multiplying the tonnage of the raw sand by the calculated weight percentage of total economic mineral, (Table 5).

Table 3: The frequencies of economic minerals in the naturally highly concentrated black sands.

Frequency of economic minerals (%)											
Magt. %	Ilmenite (%)				Gar. %	Leuc. %	Zir. %	Rut. %	Mon. %	Trace %	Total %
	G1	G2	G3	Total							
11.61	5.97	23.92	3.85	33.74	2.88	2.58	4.11	1.26	0.05	0.005	56.23

Table 4: Volume, apparent density and tonnage of the raw sand of studied sectors.

Studied Sectors	Volume (m^3) (length x width x depth)	App. Density of raw sands (ton/m^3)	Tonnage of raw sand (tons)
Southern sector	10000 x1000 x1= 10,000000	1.59	15,900000
Northern sector	10000 x1000 x1= 10,000000	1.60	16,000000
High. con. black S.	2500 x20 x0.3= 15,000	1.70	25,500

Table 5: Reserves of total economic minerals in studied sectors.

Studied sectors	Tonnage of raw sand (tons)	Average economic minerals content wt.%	Reserve of total economic minerals (tons)
Southern sector	15900000	3.47	551,014.5
Northern sector	16000000	4.71	753,600
Highly Concentrated black sand	25500	56.23	14,338

The tonnage of each individual economic mineral was calculated by multiplying the tonnage of the raw sand of the studied sectors by the calculated weight percentage of each economic mineral, (Table 6).

Physical and chemical features of economic heavy minerals.

1- Magnetite, (Fe^{2+}, Fe_2^{3+} O_4).

Magnetite grains are subangular to subrounded beside octahedron particles with contact double twins and parting plains, (Fig. 7).

A trace of highly magnetic particles nearly have abnormal shapes (spherical, drop like, cocoon like, elongated, ovoid and discoidal) and composed mainly from iron oxide were detected in magnetite concentrate, (Fig. 8).

The grain size distribution of the magnetite in the study area is a unimodal distribution with modal class lies in the very fine sand size class which constitutes more than 93% of the particles. The fine sand size class contains 5.21% from the particles. This close grain size distribution is an important parameter for physical separation processes. Complete euhedral and spherical grains of magnetite were picked from magnetite concentrate using binocular stereomicroscope and subjected to oxides analyses using Environmental Scanning Electron Microscope. The average contents of major oxides in the analyzed euhedral magnetite grains are shown in (table 7).

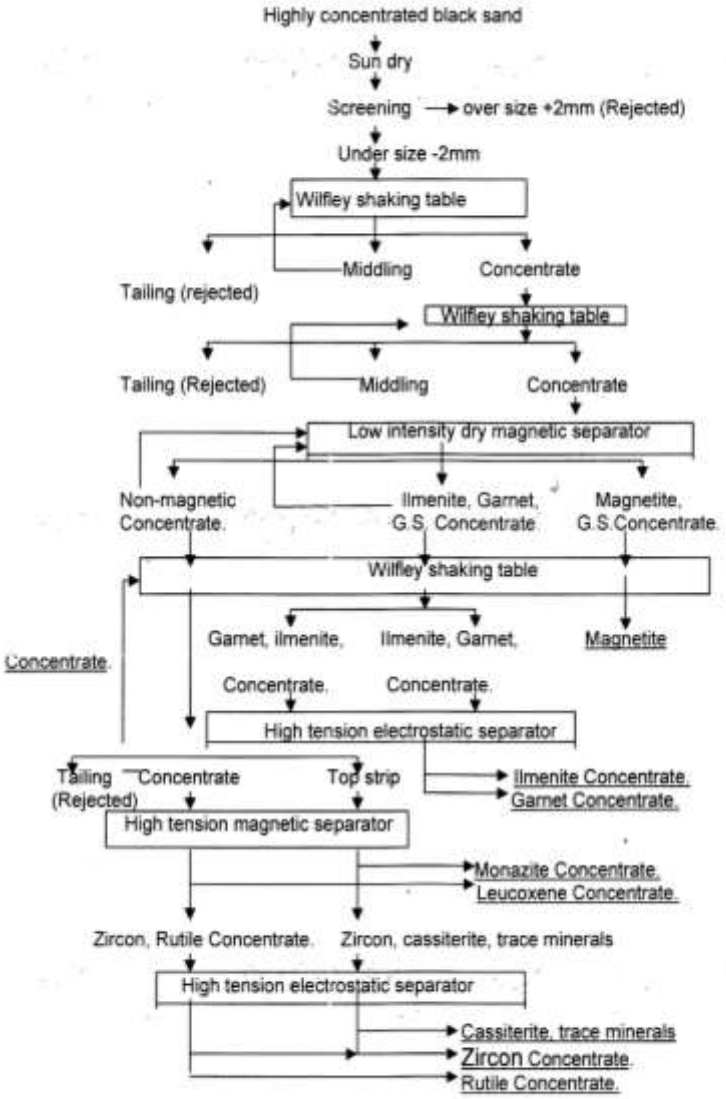

Fig. 6: The different steps of the flowsheet used for concentrating and separating the Egyptian beach economic minerals concentrate.

Table (6): The average content (Av. cont., Wt. %) and reserve tonnage for each economic mineral in the studied sectors.

Economic mineral	Southern coastal plain sector		Northern coastal plain sector		Naturally highly concentrated black sand	
	Av .cont. wt.%	Reserve (tons)	Av .cont. wt.%	Reserve (tons)	Av .cont. wt.%	Reserve (tons)
Magnetite	1.13	179,670	1.63	260,800	11.61	2,960.55
Ilmenite	1.96	311,640	2.53	404,800	33.74	8,603.70
Garnet	0.13	20,670	0.19	30,400	2.88	734.40
Leucoxene	0.08	12,720	0.12	19,200	2.58	657.90
Zircon	0.12	19,080	0.17	27,200	4.11	1,048.05
Rutile	0.040	6,360	0.06	9,600	1.26	321.30
Monazite	0.0055	874.5	0.01	1,600	0.05	12.75
Total	3.47	551,014.5	4.71	753,600	56.23	14,338.65

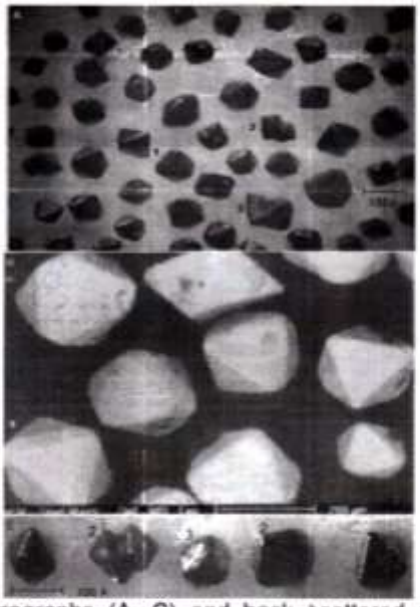

Fig. 7: Stereomicrographs (A, C) and back scattered electron image (B) showing octahedron crystals, composite crystal (1), contact double twins (2) and triangle parting plains in magnetite crystals (3).

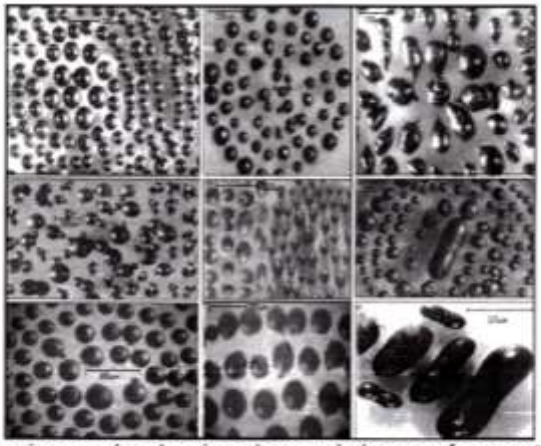

Fig. 8: Stereo micrographs showing abnormal shapes of magnetite (spherical, drop like, cocoon like, elongated, ovoid and discoidal).

2- Ilmenite, $FeTiO_3$.

The formula of ilmenite may be more fully expressed as (Fe, Mg, Mn) TiO_3. Ilmenite represents the main constituent in the heavy economic minerals of the Egyptian black sand deposits. Its particles are predominantly sub-rounded to well rounded while complete euhedral particles were detected. Under the binocular microscope, ilmenite occurs as deep blue to black rounded to subrounded grains with metallic to submetallic luster. According to the degree of alteration, the colour of ilmenite and their alteration product change from black to grey to white (Fig. 9).

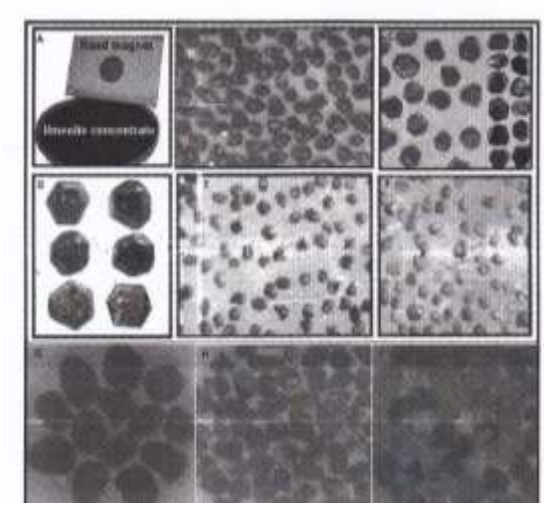

Figure 9: Stereomicrographs showing, ilmenite concentrate (A), subrounded black ilmenite grains (B, ×40), euhedral ilmenite grains (C, ×45), coarse euhedral ilmenite grains (D, ×80), altered ilmenite (E, ×40), leucoxene grains (F, ×40), polished section of homogenous ilmenite (G, ×80), polished section of altered ilmenite (H, ×45), polished section of leucoxene (I, ×45).

The colour of altered ilmenite is variable, black, dark brown, light brown, light grey, reddish, orange, yellow and white, (Fig. 10). According to Temple (1966) the inherent colour of altered ilmenite grains is directly depends on the degree of alteration and TiO_2 content.

Lucoxination process does not only affect the overall grade, but also changes the density of mineral grains (Temple, 1966) and their magnetic susceptibility (Frost et al. 1986). Both SiO_2 and Al_2O_3 impurity levels in the grains increase with increasing leucoxination process (Hugo and Cornell, 1991). In current usage leucoxene generally refers to a commercial concentrate rich in titanium dioxide (>70%) and it is a mixture of pseudorutile and rutile (Frost et al., 1983). Residual particles of ilmenite being enclosed in many of the altered ilmenite grains and a few grains still preserved with the crystal form of parent ilmenite, (Fig. 11).

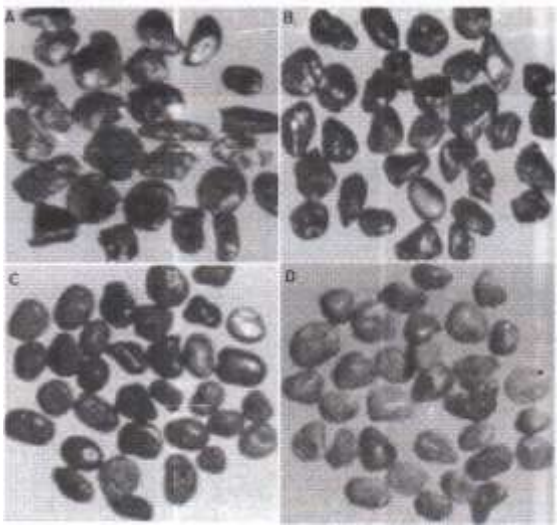

Figure 10: Stereo micrographs showing, A) Black altered ilmenite grains (×80). B) Dark brown altered ilmenite grains (×80). C) Light brown ilmenite grains (×80). D) White altered ilmenite grains (×80).

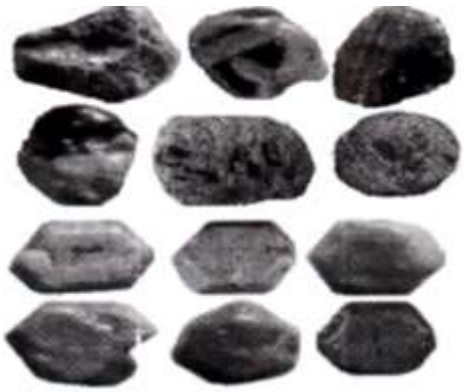

Figure 11: Stereomicrograph showing residual ilmenite particles within altered ilmenite grains and a few grains still preserved with the crystal habit of the parent ilmenite grains (×100).

The price of the world marketable ilmenite concentrates depends on its grain size (Industrial Mineral Magazine, 2003) is important factor (Fouda et al., 2010) during chemical treatment and upgrading of ilmenite. The grain size distribution of the studied ilmenite and altered ilmenite lies in the very fine sand size class constitutes more than 89%

and 80% of the particles respectively. The fine sand size class represents about 10.46 % and 18.33% from the particles respectively.

Euhedral and altered ilmenite grains were selected by picking process using binocular stereomicroscope. They were subjected to oxides analyses using Environmental Scanning Electron Microscope. The Energy Dispersive X-ray and the back scattered electron image were graphically represented in Figures (12&13) and the chemical composition of these grains are given in (Table 8).

1- Garnet minerals

The bulk garnet concentrate of study area is dominated by the pink and red types constituting about 90% of the garnet concentrate. Several colour varieties were also observed under the binocular stereomicroscope such as yellow, black, colourless, and green. Garnet grains are represented by angular (49%), sub-spherical (45%), spherical (5%) and euhedral grains (1%) as (rhombic dodecahedron, trapezohedron, composite crystals and twins), Fig. (14). Lower frequency of spherical grains in the garnet concentrate may be related to the mineral processing techniques. During wet table concentration, spherical grains are rolling easier than other shapes (Pettijohn, 1975; Burt, 1984 and Jones, 1987). So, a considerable amount of spherical garnet escapes in wet table tail fractions. Also, a considerable amount of garnets is removed during electrostatic separation of garnet from ilmenite due to the high centrifugal force of spherical garnet grains.

Table 8: The average contents of major oxides in euhedral and spherical ilmenite grains.

Oxide	Iron oxide	TiO_2	MnO_2	Cr_2O_3	V_2O_3	MgO	CaO	SiO_2	Al_2O_3	K_2O	SO_3
Aver.of Euhed. Gr.	46.10	47.18	1.22	0.51	0.12	1.1	0.22	2.13	0.91	0.19	0.33
Aver. Of altered Gr.	5.42	89.72	0.75	0.25	0.00	0.00	0.32	3.33	0.29	0.00	0.00

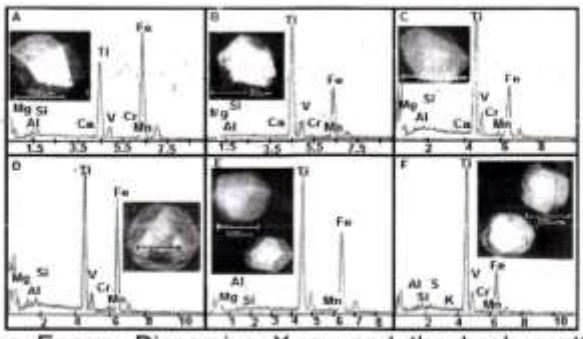

Figure 12: The Energy Dispersive X-ray and the back scattered electror image of six ilmenite euhedral grains.

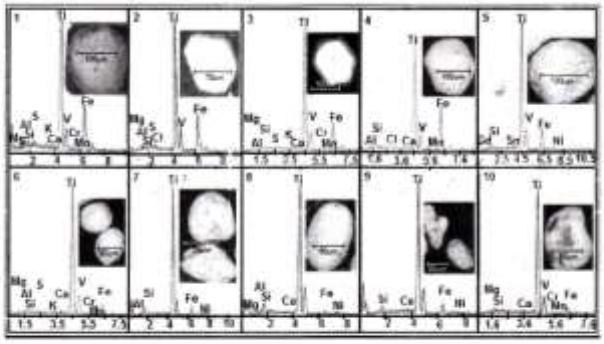

Figure 13: The Energy Dispersive X-ray and the back scattered electron image of ten altered ilmenite grains.

Garnet grains which contain inclusions represent about 10% of the garnet concentrate. These inclusions are represented by, black, red and colourless inclusions. These inclusions were identified previously by Massoud, 2003 and Abu-Halawa, 2005 to be, magnetite, ilmenite, zircon, rutile and quartz inclusions. Quartz constitutes most of the inclusions in garnet grains which may be the main reason for the lower density of the bulk garnet concentrate. The end use of garnet grains depends on their grain size, to be graded according to size distribution. The grain size distribution of the garnet is a unimodal distribution with a mode lies in the fine sand size class which constitutes more than70.78% of the particles. The medium sand size class contains 18.30% from the particles. It is noticed that garnet has a coarse grain size relative to other heavy minerals in the studied samples. The picked euhedral garnet grains were subjected to oxides analyses using Environmental Scanning Electron Microscope. The Energy Dispersive X-ray and the back scattered electron image were graphically represented in (Fig. 15) and the chemical composition of these grains are given in (Table 9).

This wide variation in garnet chemistry determines many of their physical properties. As an example, the calcium garnets generally have a lower specific gravity, a lower hardness and are typically green in colour. In contrast, the iron and manganese garnets have a higher specific gravity, a greater hardness and are typically red in colour. 4- Zircon mineral, (zirconium silicate, ZrSiO4). Zircon grain habits show euhedral crystals (short or long prismatic bipyramidal crystals, octahedral crystals, rhombic dodecahedron crystals) or irregular, spherical, ovoid and elongated grains. There is no distinct cleavage, and the mineral breaks with a concoidal fracture. It is usually colourless, red, brown, yellow, grey, pink and green in colour, (Fig. 16). The element zirconium (Zr) is chemically very similar to the hafnium element (Hf) and is always built into the crystal lattice of the mineral zircon. The content of HfO_2 in zircon averages 0.5-2.0 % by mass. Zircons with increased contents of up to 24 % Hf are called alvites in mineralogical terms. Naegite, however, is a zircon with increased Y, Nb and Ta contents. The colourless zircon represents about 85% of the zircon concentrate of the studied area. Zircon grains with yellowish to dusky colours constitute about 10% and the remaining 5% include orange, red, brown, pink and green zircon varieties.

Table 9: The average contents of major oxides in euhedral garnet grains.

Oxide	Iron oxide	TiO_2	MnO	Cr_2O_3	Na_2O	MgO	CaO	SiO_2	Al_2O_3	K_2O	SO_3
Maximum	72.72	12.76	18.69	0.65	3.30	15.85	31.81	46.77	33.07	0.68	0.93
Minimum	5.54	0.00	0.00	0.00	0.00	0.00	0.00	13.80	8.54	0.00	0.00

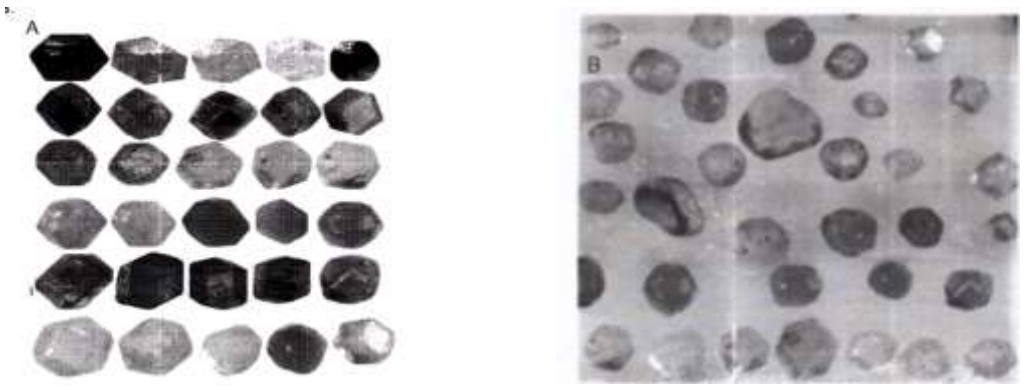

Figure 14: Stereomicrographs showing, A-Complete euhedral garnet crystals of different colour, (×80), B-Irregular, spherical, euhedral garnet grains of different colour, (×50).

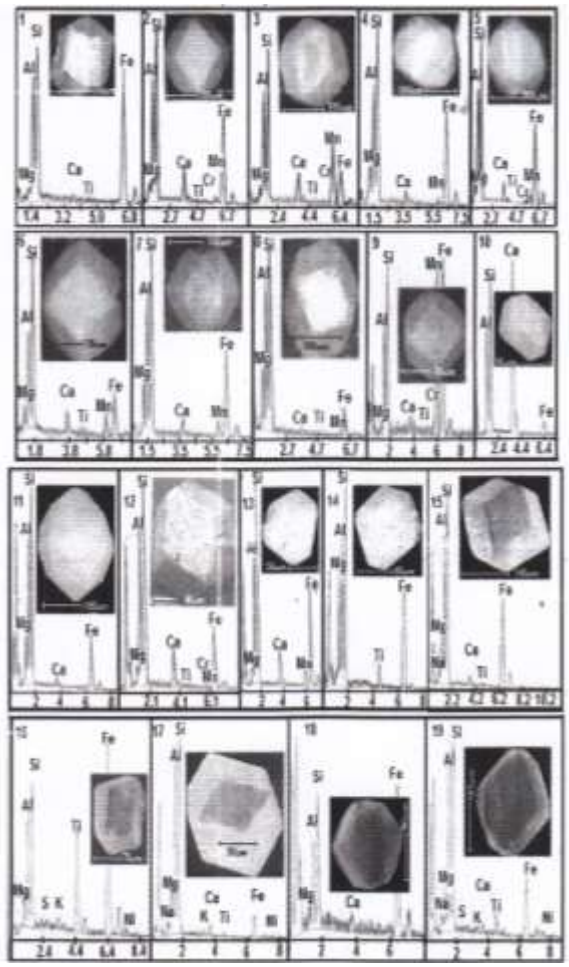

Fig. 15: The Energy Dispersive X-ray and the back scattered electron image of nineteen euhedral garnet grains.

Zircon is a typical placer mineral since it accumulates due to its weathering resistance and high apparent density. This does not apply to metamictic zircons that are unstable because of their physically disrupted crystal lattices. Therefore, these are rarely found in placers and are as a consequence also rare in commercial zircon concentrates.

The magnetic zircon fraction which was obtained from the bulk zircon concentrate is particularly rich in coloured grains. The coloured grains represent about 70%, of this magnetic zircon fraction. The most common colours are red and brown with some malacons. The reddish-brown colour may be due to iron oxide stains. So, to eliminate of the coloured zircon grains by high intensity magnetic separators as a magnetic fraction reduces the amount of coated grains.

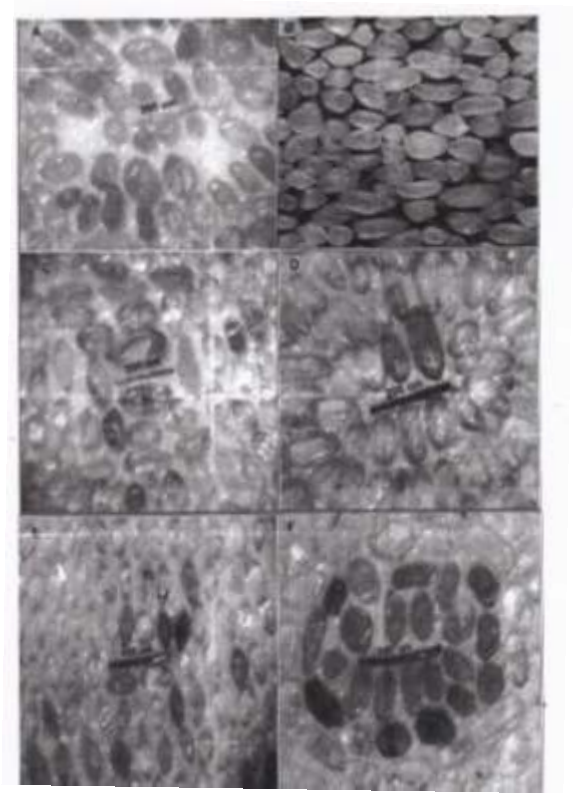

Fig. 16: Stereo micrographs showing, pink, colourless, Red, Yellow, and brown zircon with different crystal habits (irregular, euhedral crystals, ovoid, and platy grains.

The grain size distribution of the zircon is unimodal with a very fine sand size modal class which constitutes more than 97% of the particles. The fine sand size class is only 1.31% from the particles.

The picked zircon grains subjected to oxides analysis using Environmental Scanning Electron Microscope. The Energy Dispersive X-ray and the back scattered electron image were graphically represented in Fig. (17) and the chemical composition of these grains are given in Table (10).

Radioactivity of zircon concentrate is very important to meet market specification. The market specification limit of radioactivity of zircon which is used in domestic purposes such as ceramics is U+Th < 500 ppm (Elder and Domenico, 2000).

So, elimination of this magnetic zircon fraction (by high intensity magnetic separator) is very important to reduce the contents of Fe and radioactive elements from the high grade zircon concentrate. This is necessary to meet the world market specifications.

Table (10): The average contents of major oxides in selected zircon grains.

Oxide	Zr+Hf Oxide	Iron oxide	TiO_2	MnO	Cr_2O_3	RE_2O_3	MgO	CaO	SiO_2	Al_2O_3	ThO_2	UO_2
Aver.	64.47	0.75	0.47	0.12	0.11	3.30	0.55	o.22	31.37	0.35	0.68	0.93

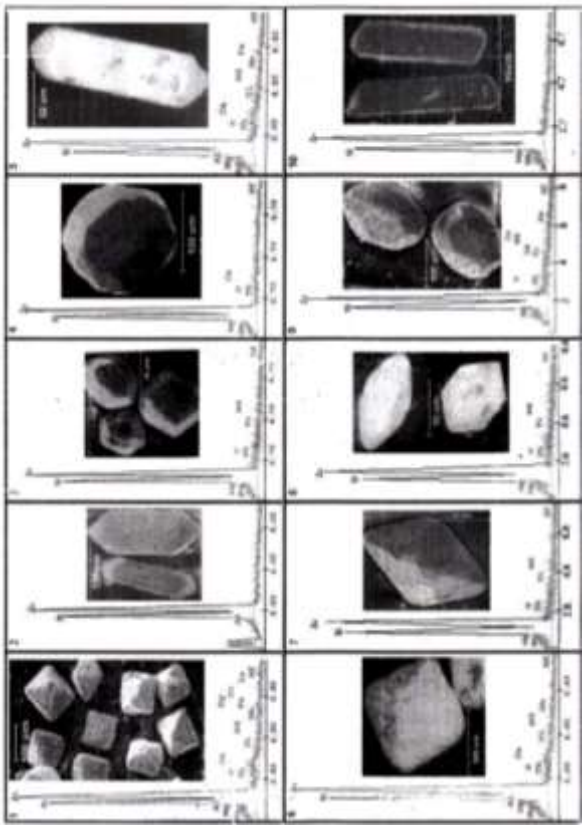

Fig. (17): The Energy Dispersive X-ray and the back scattered electron image of selected twenty zircon grains.

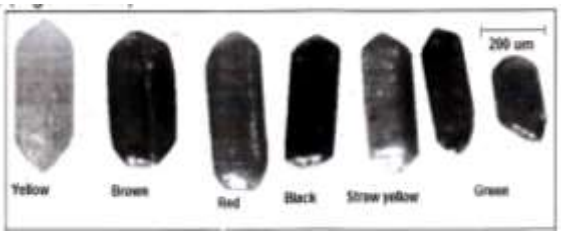

Fig. (17): Stereomicrograph showing rutile grains colours.

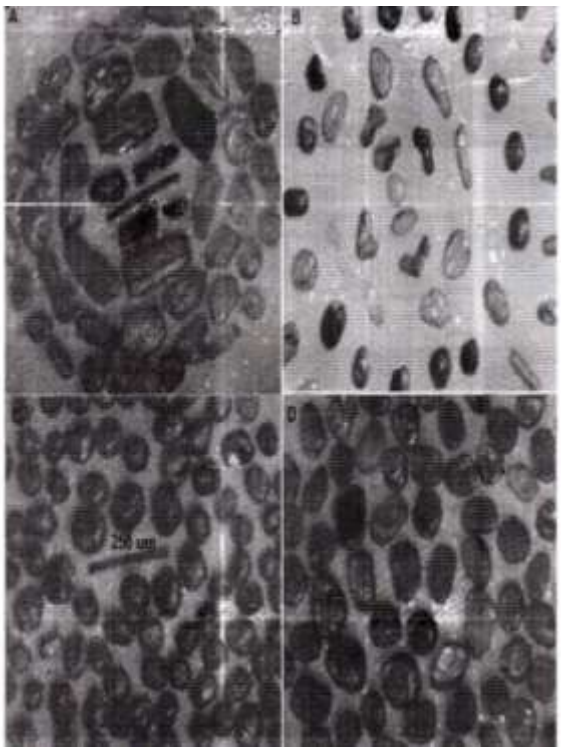

Fig. 18: Stereomicrographs showing prismatic, platy, spherical and discoidal rutile grains with different colours (yellow, red. black and deep green)

5- Rutile mineral, TiO_2

The rutile grains vary from transparent to black opaque grains, both transparent and translucent grains exhibited a wide range of colouration according to their chemical components particularly trace elements. The colours of rutile are reddish brown varities constituting about 60%, of the rutile concentrate, black and yellow constituting 30% and 10% and straw yellow and green. This variation in colour is due to the impurity ions in the crystal structure, especially the ferric iron, niobium and tantalum. Twinning is very common in rutile as knee shaped twins, V-shaped twins, cross twins and fish tail twins, (Figs. 17&18).

The Egyptian beach rutile is represented by tow main varieties, the primary rutile formed during magmatic crystallization and secondary rutile derived from the alteration of Fe-Ti oxides especially ilmenite. The secondary rutile is the end product of the alteration of Fe-Ti oxides and is characterized by its black opaque appearance under the polarized microscope. Anwar and El- Bouseily (1970, part II) reported some grains of secondary rutile are observed enclosing opaque mineral (ilmenite) indicating

to be derived from the latter by alteration process.

Generally, most of the rutile grains, about 70% are subrounded to well rounded;. The tabular rutile grains are represented by about 20% whereas the angular to subangular grains constitute about 10%. Completely developed euhedral crystals of rutile are rare. When encountered they are represented by bipyramidal tetragonal prisms.

The grain size distribution of rutile lies in the very fine sand size class which constitutes more than 92% of the particles. The fine sand size class constitutes 7.17% from the particles.

The picked rutile grains of different colours and shapes were subjected to oxides analyses using Environmental Scanning Electron Microscope. The chemical composition of these grains are given in Table (11) and the Energy Dispersive X-ray and the back scattered electron image were graphically represented in (Fig. 19).

Table (11): The average contents of major oxides in selected rutile grains.

Oxide	TiO_2	SnO_2	Iron oxide	Cr_2O_3	PbO_2	K_2O	SO_3	Gd_2O_3	NiO
Aver.	95.32	0.84	1.27	0.53	0.96	0.07	0.32	o.34	0.33

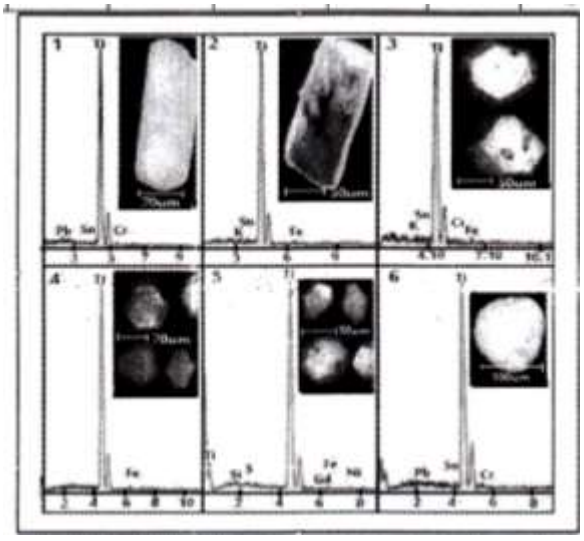

Fig. 19: The Energy Dispersive X-ray and the back scattered electron image of six rutile grains.

6- Monazite mineral, (Ce, La, Nd, Pr, Th, Y) PO_4,

Monazite is radioactive due to the presence of thorium and, less commonly, uranium. Monazite is a honey yellow, yellowish brown, reddish brown, greenish brown, grey or colourless mineral with a resinous to vitreous luster. It is translucent and rarely seen in large grains or as well-formed crystals. Granular masses are sometimes seen where monazite is locally abundant. Cerium is the most common rare earth element in monazite-(Ce), and so forth. Silica (SiO2) is present in trace amounts, as well as small amounts of uranium and thorium. Due to the alpha decay of thorium and uranium, monazite contains a significant amount of helium, which can be extracted by heating.

The crystal habits (prismatic bipyramidal, octahedron, ovoid, spherical, discoidal and contact twins) and colours (yellow, red, brown, grey, orange and green) of monazite grains are shown in (Fig. 20). Many monazite grains contain red, black, grey and colourless inclusions.

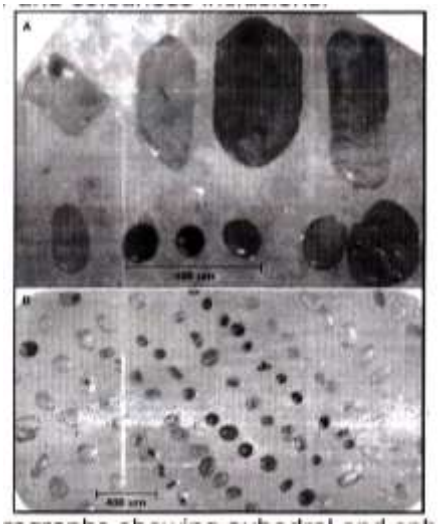

Fig. 20: Stereomicrographs showing euhedral and spherical grains of monazite with different colours.

The grain size of the monazite mineral lies in the very fine sand size class (more than 98%) of the particles. The fine sand size class is about 0.25% from the particles whereas 1.50 % of monazite lies in the coarse silt size The picked monazite grains of different colours and shapes were were subjected to oxides analyses using Environmental Scanning Electron Microscope. The chemical composition of these grains are given in (Table 12) and the Energy Dispersive X-ray and the back scattered electron image were graphically represented in (Fig. 21).

Table 12:The average contents of major oxides in selected monazite grains.

Oxide	P_2O_5	Ce_2O_3	La_2O_3	Nda_2O_3	Sm_2O_3	Gd_2O_3	Eu_2O_3	$Y2O_3$	Sc_2O_3	Pr_2O_3	Pm_2O_3	Tm_2O_3
Aver.	27.66	29.77	14.23	11.54	2.82	1.92	0.24	o.17	o.13	0.37	0.70	0.25
Oxide	Yb_2O_3	Dy_2O_3	ThO_2	U_3O_8	AtO_2	SiO_2	CaO	Fe_2O_3	MgO	Pb_2O_3	Al_2O_3	Total
Aver.	0.63	0.02	6.12	1.16	o.1o	o.68	0.80	0.20	0.10	0.21	0.17	99.99

7- Cassiterite mineral, SnO_2

Cassiterite is represented mostly by prismatic bipyramidal grains. Crystal twinning is common in cassiterite; the typical twin is bent at a near 60 degree angle, forming an "elbow twin". A cassiterite grain colour varies between black, brownish black, reddish brown, red, yellow, grey, white; rarely colorless when it is pure, (Fig. 22).

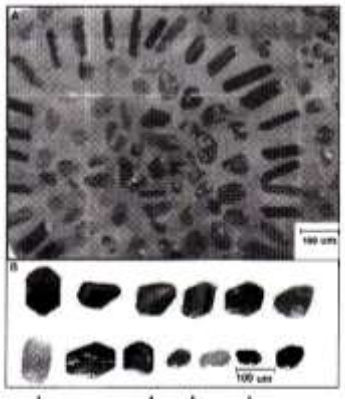

Fig. 22: Stereomicrograph showing cassiterite grains.

Some grains of cassiterite were picked from cassiterite concentrate using binocular stereomicroscope and subjected to oxide analyses using Environmental Scanning Electron Microscope. The oxide chemical compositions of the analyzed grains are shown in Table (13) and the Energy Dispersive X-ray and the back scattered electron image were graphically represented in Fig. (23).

Table (13): The average contents of major oxides in selected cassitierite grains.

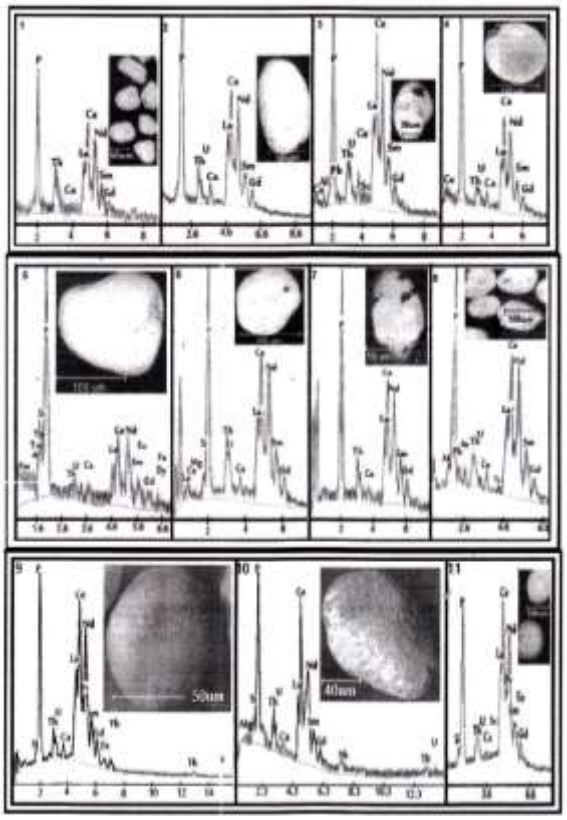

Fig. 21: The Energy Dispersive X-ray and the back scattered electron image of eleven monazite grains.

The grain size of the cassiterite mineral lies in the very fine sand size class constituting more than 88% of the particles. The fine sand size class contains 0.21% from the particles whereas about 11.57 % of cassiterite lies in the coarse silt size. The dark coloured and black cassiterite grains are coarser than the light coloured cassiterite grains.

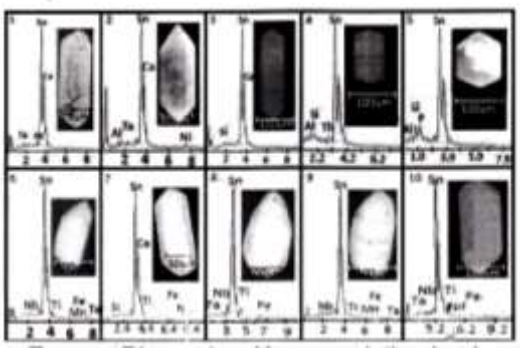

Fig. (23): The Energy Dispersive X-ray and the back scattered electron image of cassiterite grins.

Some rare economic minerals detected in cassiterite concentrate as: Gold grains, Fig. (24), Copper grains, Fig. (25), Lead grains, Fig. (26), Galena, Fig. (27), Bismuthinite Bi2S3, Fig. (28), Cinnabar HgS, Fig. (29), Tin and mercury spherical grains, Fig. (30), Sperrylite mineral, Pt As2, Fig. (31), PGES minerals, Fig. (32) and Silver grains, Fig. (33).

Table (13):The average contents of major oxides in selected cassitierite grains.

Oxide	SnO_2	TaO	Nb_2O_5	TiO_3	FeO	MnO	AcO_2	CaO	Al_2O_3	NiO	SiO_2	ThO_4	P_2O_5
Aver.	96.75	0.78	0.32	0.35	0.29	0.08	0.10	o.47	o.37	0.20	0.15	0.10	0.04

1- Gold grains.

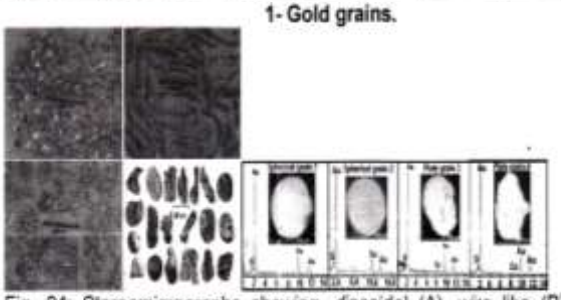

Fig. 24: Stereomicrographs showing, discoidal (A), wire like (B) and platy ornamented gold grains (C) and the back scattered electron image of the analyzed gold grains.

2-Copper grains.

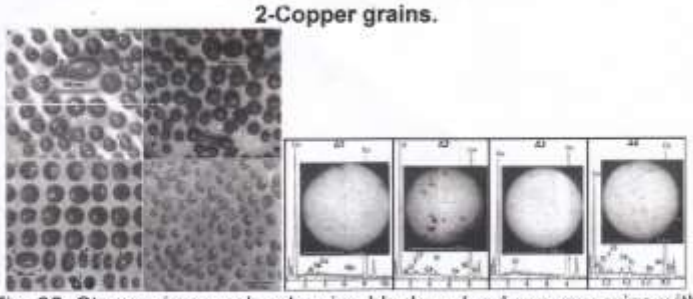

Fig. 25: Stereomicrographs showing black and red copper grains with different grain habits as, spherical (most of grains), ovoid (2), drop like (3), elongated (4) and cocoon like (5) and the back scattered electron image of the analyzed copper grains.

3 - Lead grains.

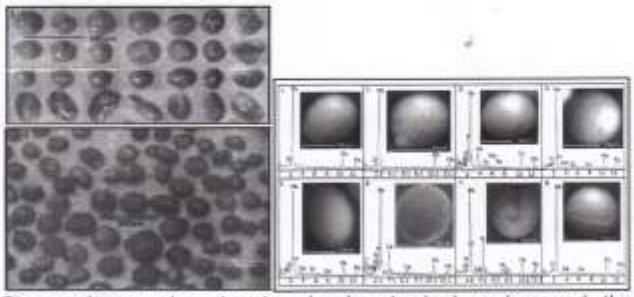

Fig. 26: Stereomicrographs showing lead spherical grains and the back scattered electron image of the analyzed spherical lead grains.

4 – Galena.

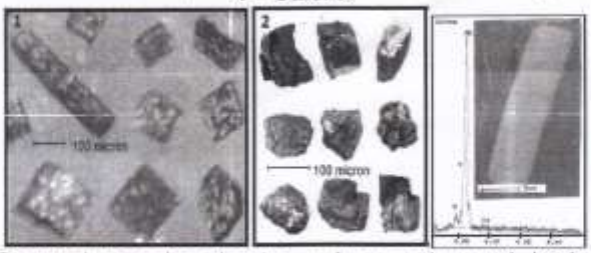

Fig 27: Stereomicrographs showing galena grains and back scattered electron image of galena grain.

5 - Bismuthinite (Bi_2S_3).

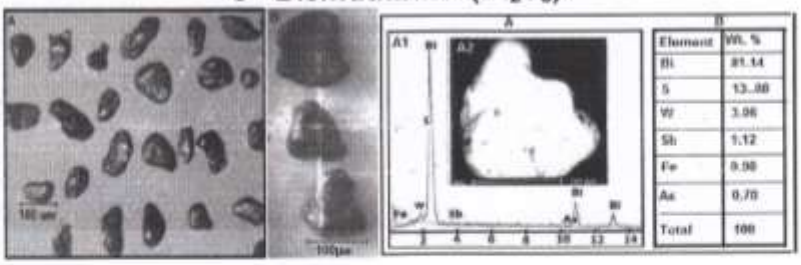

Fig. 28: Stereomicrographs showing bismuthinite grains and the back scattered electron image (A) of the analyzed bismuthinite grain.

6 - Cinnabar HgS.

Fig. 29: Stereomicrograph showing cinnabar grains and the back scattered electron image of analyzed cinnabar grain.

7 -Tin and mercury spherical grains.

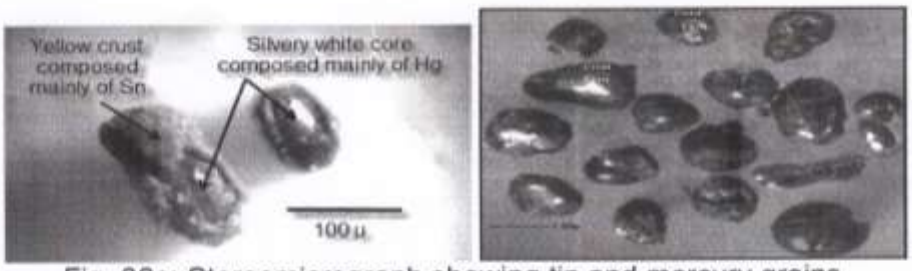

Fig. 30a: Stereomicrograph showing tin and mercury grains.

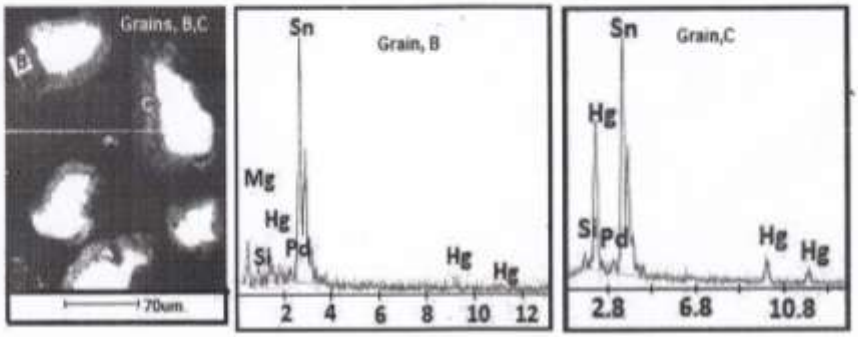

Fig. (30b): The Energy Dispersive X-ray and the back scattered electron image of the analyzed tin and mercury grains, (B, C).

8 - Sperrylite mineral, $PtAs_2$.

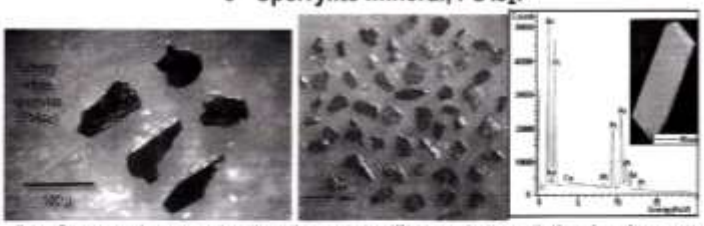

Fig. 31: Stereomicrograph showing sperrylite grains and the back scattered electron image of the analyzed sperrylite grain.

9- PGE_S minerals.

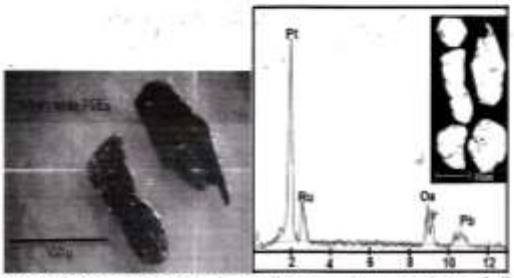

, Fig. 32: Stereomicrograph showing silvery white grains of PGE_S and the back scattered electron image of the analyzed PGE_S grain.

10- Silver grains.

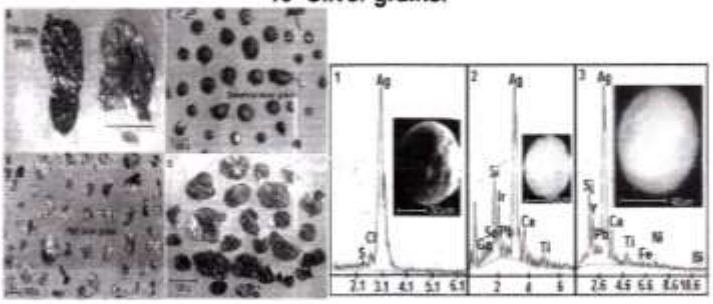

Fig. 33: Stereomicrographs showing platy (A, B, D) and spherical silver grains (C) and the back scattered electron image of the analyzed silver grains.

SUMMARY AND CONCLUSION

Geomorphology and mineralogy of the top meter black sands north west of El-Burullus Lake, Kafr Al-Sheikh Governorate, Egypt are the main goals of the present study. The study area lies on the Mediterranean Sea Coast, about 8Km east of Rosetta distributary mouth, north-west of El- Burullus lake between Longitudes 30˚ 25' 48" - 30˚ 33' 00" E and Latitudes 31˚ 26' 42" - 31˚ 27' 18" N. It covers an area of about $20Km^2$, with 10Km long parallel to the shoreline and two kilometers width nearly perpendicular to the shoreline.

El-Sahel (coastal) drain which runs parallel to the shoreline divides the coastal plain of study area into northern and southern sectors; each sector covers an area of about $10Km^2$. The northern sector is characterized by relatively highly concentrated black sand especially in the near shore area. The southern sector is characterized by diluted homogenous sediments compared with the northern sector.

Due to many factors as, the construction of water control structures along the Nile River and natural reduction of Nile floods, the shoreline suffered from severe erosion especially in the seaward protruding areas especially Rosetta headland. The total eroded longitudinal distance between, 1922 shoreline and the eastern sea wall was estimated to be

about 5 Km. The eroded sediments from the promontory was carried by the long shore current and redeposited in areas of shoreline accretion at Abu-Khashabah beach (about 8 Km east of Rosetta mouth).

In order to protect the eastern side of Rosetta headland, a sea wall was constructed during 1989-1991 east the Rosetta mouth and parallel to the shoreline. The down drift side of the eastern seawall is affected greatly by erosion and retreat of the shoreline, so, a set of five groins were constructed since 2003 to minimize the shore erosion and stabilize the eastern bank of the promontory. These groins are built perpendicular to the shoreline to trap moving sand and widen the beach. The lengths of these groins vary between 400 and 500 meters and spaced 800 to 900 meters apart. The recently highly concentrated black sands formed along the beach face east of the fifth groin to about 500m east of the guard station number 63; indicate the changing of the western part of Abu-Khashabah beach from zone of accretion to zone of erosion.

Rate of shoreline retreat along Abu-Khashabah beach in front of El-Matlaa Medak was 43.66 m/y in the time interval between 2003 and 2012. To retreat erosion process along Abu-Khashabah beach, four groins must be added eastward from the last groin to reach to the widest coastal plain area, far from the river bend at Abu-Khashabah village. Generally, the months, July, August and September are recommended for constructing the protective engineering structures.

Along the shoreline of the study area, erosion and accretion phenomena is indicated by the presence of alternation of highly concentrated and low concentrated sediments, distribution of flaky, discoidal, spherical stones and mud balls. The north-western part of the northern coastal plain sector of the study area is characterized by the distribution of highly concentrated black sands which extend from the fifth groin eastward about 3.5 Km. These deposits are affected greatly by a wave cut along the shore line.

The coastal plain of study area was covered by 561 samples to a depth of one meter at the intersection of a grid pattern 200m×200m nearly parallel and perpendicular to the shoreline. The northern sector of coastal plain area is covered by 255 samples whereas the southern sector is covered by 306 samples. Naturally highly concentrated black sands are deposited in a thin mantle near and parallel to the shoreline of the northern coastal plain sector. The highly concentrated black sands were scraped from the mantle to a depth of about 30 cm. The collected sands were stored in an open store at Abu-Khashabah site where a processing pilot plant was constructed.

Concentration and separation of economic heavy minerals using physical ore dressing technique is considered closer to reality; cheaper and safe from a health point than the heavy fluid technique.

The average content (Av. cont.) and reserve tonnage for each economic mineral in the studied sectors are: magnetite has an average content 11.61% with a reserve 296055 ton, lmenite has an average content 33.74% with a reserve 860370 ton, garnet has an average content 2.88% with a reserve 73440 ton, leucoxene has an average content 2.58% with a reserve 65790 ton, zircon has an average content 4.11% with a reserve 104805 ton, rutile has an average content 1.26% with a reserve 3210 ton and monazite has an average content 0.05% with a reserve 1275 ton with a total average of economic minerals 56.23% and reserve of 1433865 tons.

The Egyptian black sand magnetite grains exhibit dull black to brownish black in colour, the brownish tint can be attributed to their alteration and/or oxidation process, in addition to the probable presence of exsolved ilmenite and /or hematite. Magnetite grains have generally irregular shape where subangular and subrounded particles are present beside octahedron particle, contact double twins and parting plains are also present. A trace of highly magnetic particles nearly have abnormal shapes (spherical, drop like, cocoon like, elongated, ovoid and discoidal) and composed

mainly of iron oxide detected in magnetite concentrate.

The grain size distribution of the magnetite in the study area is a unimodal distribution with modal class lies in the very fine sand size class which constitutes more than 93% of the particles.

The average contents of major oxides in the analyzed magnetite grains are shown as follows,

Oxide	Iron oxide	TiO_2	MnO_2	Cr_2O_3	V_2O_3	MgO	CaO	SiO_2	Al_2O_3
Average	86.39	6.20	0.85	0.56	0.56	1.51	0.58	3.25	1.09

Ilmenite represents the main constituent in the heavy economic minerals of the Egyptian black sand deposits. Its particles are predominantly sub-rounded to well rounded while complete euhedral particles were detected. The colour of ilmenite and their alteration product changes from black to grey to white according to the degree of alteration.

The grain size distribution of the studied ilmenite and altered ilmenite, shows that they have a unimodal grain size distribution with the modal class lies in the very fine sand size class which constitutes more than 89% and 80% of the particles respectively. The fine sand size class contains about 10.46 % and 18.33% from the particles respectively.

The major oxides chemical analysis of fresh and altered ilmenite are shown as follows,

Oxide	Iron oxide	TiO_2	MnO_2	Cr_2O_3	V_2O_3	MgO	CaO	SiO_2	Al_2O_3	K_2O	SO_3
Aver.of Euhed. Gr.	46.10	47.18	1.22	0.51	0.12	1.1	0.22	2.13	0.91	0.19	0.33
Aver. Of altered Gr.	5.42	89.72	0.75	0.25	0.00	0.00	0.32	3.33	0.29	0.00	0.00

Generalized chemical composition of garnet is $A_3\ B_2\ (SiO_4)_3$. In that composition A can be Ca^{2+}, Mg^{2+}, Fe^{2+} or Mn^{2+}, and B can be Al^{3+}, Fe^{3+}, Mn^{3+},

V^{3+} or Cr^{3+}. The bulk garnet concentrate of study area is dominated by pink and red colours. Several colour varieties were observed under the binocular stereomicroscope (pink, red, yellow, black, Colourless, and green). Pink and red garnet varieties constitute about 90% of the garnet concentrate. The grain size distribution of the garnet is a unimodal distribution with a mode lies in the fine sand size class which constitutes more than70.78% of the particles. The medium sand size class contains 18.30% from the particles. It is noticed that garnet has a coarse grain size relative to other heavy minerals in the studied samples. The major oxides chemical analyses were applied on the hand-picked euhedral garnet grains with different colours. Because the examined garnets have very small contents of Cr, uvarovite is considered insignificant. The garnets contain major Al, Fe, Mn and minor Mg and Ca. Thus the garnet grains are represented mainly by almandine ($Fe_3Al_2Si_3O_{12}$), as a major component and spessartine ($Mn_3Al_2Si_3O_{12}$), pyrope, ($Mg_3Al_2Si_3O_{12}$) and grossularite ($Ca_3Al_2Si_3O_{12}$) as minor components. Zircon (zirconium silicate, $ZrSiO_4$) grain habits show euhedral crystals (short or long prismatic bipyramidal crystals, octahedral crystals, rhombic dodecahedron crystals) or irregular, spherical, ovoid and elongated grains. There is no distinct cleavage, and the mineral breaks with a concoidal fracture. It is usually colourless, red, brown, yellow, grey, pink and green in colour. The colourless zircon represents about 85% of zircon concentrate. Zircon grains with yellowish to dusky colours constitute about 10% and the remaining 5% include orange, red, brown, pink and green zircon varieties. The grain size distribution of the zircon is a unimodal distribution with a modal class lies in the very fine sand size class which constitutes more than 97% of the particles. The fine sand size class contains 1.31% from the particles. The Environmental Scanning Electron Microscope of zircon shows that the content of (Zr+Hf) O_2 ranges from 60.09% to 68.62% with an average value 64.47%. The percent of SiO_2 ranges from 25.70% to 35.66% with an average 31.37%. Thorium oxide content ranges from 0.00% to 0.86% with an average 0.37% while the UO_2 content ranges from 0.00% to 0.87% with an average 0.40%. The Egyptian black sand rutile is mostly prismatic, tabular, discoidal and sometimes spherical. The colour

of rutile is yellow, brown, red, black, straw yellow and green. This variation in colour is due to the impurity ions in the crystal structure, especially the ferric iron, niobium and tantalum. Twinning is very common in rutile as knee shaped twins, V-shaped twins, cross twins and fish tail twins. The reddish brown variety constitutes about 60% of the rutile concentrate. Black and yellow rutile grains constitute about 30% and 10%; respectively. Prismatic green rutile grains are detected in rutile concentrate but it is very rare. The grain size distribution of the rutile is a unimodal distribution with modal class lies in the very fine sand size class which constitutes more than 92% of the particles. The fine sand size class contains 7.17% from the particles.

According to the chemical analysis of rutile grains, the content of titanium dioxide ranges between 91.67% and 97.98% with an average value 95.32%.

Rutile concentrates with about 94% TiO_2 are consumed in some metallurgical uses. According to, the chemical data, the rutile concentrate of study area can be used in pigment industry, welding rods coating and metallurgical uses. Monazites is essentially an anhydrous orthophosphate of the cerium and lanthanum group of the rare earth elements which is represented by cerium, lanthanum, praseodymium and neodymium which reaches up to 92% of the total rare earths .The yttrium group of rare earths together with minor amounts of Ca, Mg, Mn, Fe, Al, Zr, Be and Sn occur in substitution for Ce and La only in relatively small amounts. Monazite is a honey yellow, yellowish brown, reddish brown, greenish brown, grey or colourless mineral with a resinous to vitreous luster. It is translucent and rarely seen in large grains or as well-formed crystals and has an unusually high specific gravity that ranges from 4.6 to 5.4 depending upon its composition. The grain size distribution of the monazite mineral is a unimodal distribution with a modal class lies in the very fine sand size class which constitutes more than 98% of the particles. The fine sand size class contains 0.25% from the particles whereas about 1.50 % of monazite lies in the coarse silt size. The Scanning Electron Microscope of monazite grains revealed that the Ce_2O_3 is the main REE in the studied monazite. The average weight percentage of rare earth oxides arranged as follows according to their abundance, Ce_2O_3 (29.77%) > La_2O_3 (14.23%)> Nd_2O_3 (11.54%)> Sm_2O_3 (2.82%)> Gd_2O_3 (1.92%)> Pr_2O_3 (0.37%)> Eu2O3 (0.24%), these oxides constitute more than 60 Wt.%. The average weight percentage of thorium oxide is 6.12 Wt. % whereas the average weight percentage of uranium oxide is 1.16 Wt. %. A negligible amount of radioactive minerals as xenotime, thorite, uranothorite and chevkinite, were detected in the obtained monazite concentrate.

Cassiterite is a tin oxide mineral, SnO_2. It has been the chief tin ore throughout ancient history and remains the most important source of tin today. Its colour varies between black, brownish black, reddish brown, red, yellow, grey, white; rarely colorless when it is pure. Cassiterite is represented mostly by prismatic bipyramidal grains. Crystal twinning is common in cassiterite; the typical twin is bent at a near 60 degree angle, forming an "elbow twin". The grain size distribution of the cassiterite mineral is a unimodal distribution with a modal class lies in the very fine sand size class which constitutes more than 88% of the particles. The fine sand size class contains 0.21% from the particles whereas about 11.57 % of cassiterite lies in the coarse silt size. The chemical analyses of the analyzed grains reveal clearly the considerable purity of the Egyptian beach cassiterite grains. Most of the analyzed cassiterite has SnO2 ranging between 91.70 and 98.90 wt. % with average value 96.75 wt. %, indicating that most of cassiterite grains are homogenous without obvious zoning. The average content of, TaO, Nb_2O_5, TiO_2 and FeO are 0.78, 0.32, 0.35 and 0.29 wt. % respectively.

Some rare economic minerals detected in cassiterite concentrate as, gold grains, copper grains, lead grains, galena, minium (red/yellow lead oxide), bismuthinite Bi_2S_3, cinnabar HgS, tin and mercury spherical grains, sperrylite

mineral, Pt As_2, PGES minerals and silver grains.

REFERENCES

Abdel-Fattah, M. F. (2008): Evaluation, beneficiation and mineralogy of the Egyptian beach leucoxene in Abu Khashaba area, east Rosetta, Egypt. M.Sc. Thesis, Fac.Sci. Zagazig University, Egypt.

Abu Halawa, A. (2005): Evaluation and mineral processing of some economic minerals in El Burullus – Baltim sand dunes, Nile Delta, Egypt. Ph.D. Thesis, Fac. Sci., El Mansoura University, Egypt.

Anwar, Y.M. and El-Bouseliy, A.M. (1970): Subsurface studies of the black sand deposits at Rosetta Nile mouth, Egypt. Part II, Mineralogical studies. Bull. Fac. Sci., Alexandria University, Vol. 10, pp. 141 – 150.

Burt,R.O. (1984): Gravity concentration technology. Elsevier Science Publishers B.V.,Amestrdam, the Netherlands, 605 p.

Dabbour, G.A. (1973): Physical properties and distribution of zircon in some Egyptian placer deposits. M.Sc. Thesis, Fac. Sci., Cairo University, Egypt.

Dabbour, G.A. (1980):Geological and mineralogical studies on rutile in the black sand deposits from the Egyptian Mediterranean coast. Ph.D. Thesis, Fac. Sci., Cairo University, Egypt, 155 p.

Dabbour, G.A. (1994): The Egyptian placer deposits: a potential source for Nuclear Raw Materials. 2nd Arab Conference on the Peaceful Uses of Atomic Energy, Cairo, pp. 191 – 204.

EBSCO Services Incorporated, Geelip Team (1964): Evaluation of proposed program for development of mineral deposits of Egyptian Black Sand's company. Contract AID/NESA 37, Internal report, No.1774.

Elder, J. and Domenico, J. (2000) Enhancing mineral quality through magnetic separation. Industrial Minerals, July, pp.27-33. El-Fishawi, N.M. and El Askary, M.A. (1981): Characteristic features of coastal sand dunes along El Burullus-Gamasa stretch, Egypt. Acta Mineral. Petro. Vol. 25, pp. 63 – 76.

El-Fishawi, N.M. (1984): Roundness and sphericity of the Delta Coastal sands. Acta Mineralogica-Petrographica, Szeged, Vol. XXVI, No.2, pp.235-245.

El-Hadary, A.F. (1998): Geological, sedimentological and radiometric studies on the black sand deposits, west Rosetta beach with emphasis on the heavy economic minerals. Ph.D. Thesis, Fac. Sci., Cairo Univ., Egypt.

El-Shafey, A.M. (2011): Mineralogical, evaluation and beneficiation of the economic minerals of Egyptian black sands especially Cassiterite, in Abu-Khashaba area, east Rosetta, Egypt. M.Sc. Thesis, Fac. Sci. Zagazig University.

El-Shazly, E.M. (1965): Thorium resources in the United Arab Republic and their possible utilization. Panel on utilization of Th in Power Reactors, IAEA, Vienna, pp.186-198.

Frihy, O.E.; El Fishawy, N.M.; and El Askary, M.A. (1988): Geomorphologic features of the Nile Delta coastal plain: Review Acta Adrint., 29, No. ½, 51-65.

Frost, M.T.; Grey, I.E.; Harrowfield, I.R. and Mason, K. (1983): The dependence of alumina and silica contents on the extent of alteration of weathered ilmenites from Western Australia. Mineral. Mag., Vol. 47, pp. 201-208.

Frost, M.T., Grey, I.E, Harrowfield, I.R., and Li, C. (1986): Alteration profiles and impurity element distributions of magnetic fractions of weathered ilmenite. Am. Mineral., 71, 167-175.

Fouda, M.F.; Amin, R.S.; Saleh, H.I.; Labib, A.A. and Mousa, H.A. (2010): Preparation and characterization of Nanosized titania prepared from beach black sands broad on the Mediterranean sea coast in Egypt, Via reaction with acids. Australian Journal of basic applied sciences Vol. 4 (10), pp. 4540-4553.

Hammoud, N.M.S. (1966): Concentration of monazite from Egyptian black sands employing industrial techniques. M.Sc. Thesis, Fac. Sci., Cairo University, Cairo, Egypt. 198 p.

Hammoud, N.M.S. (1975): A process for recovery of low chromium high grade ilmenite from north Egyptian beach deposits. Proc., 11th Indust. Mineral Process. Conf., Regione Autonoma Delta, Sardegna, Italy.

Hammoud, N.S. (1985): Contribution to the evaluation problems of Egyptian beach economic minerals. Annals of Geol. Sur. of Egypt, vol.15, p.45-59.

Hugo, V.E. and Cornell, D.H. (1991): Altered ilmenites in Holocene dunes from Zululand, South Africa: petrographic evidence for multistage alteration. S. Afr. J. Geol., Vol. 94, pp. 365-378.

Industrial Minerals Magazine (2003): Industrial minerals information (IM & MPW). December, p.74-75.

Jones, M.P. (1987): Applied mineralogy: a quantitative approach. Graham & Trotman Ltd., London, UK, 259p.

Massoud, S.S. (2003): Mineralogical studies for the economic minerals in the sand dunes belt at Baltim area, Egypt. Ph.D. Thesis, Fac. Sci., Ain Shams Univ., Egypt, 235pp.

Moustafa, M.I. (1999): Mineralogy and beneficiation of economic minerals in the Egyptian black sands. Ph.D. Thesis, Fac. Sci., El Mansoura University, El Mansoura, Egypt, 316 p.

Moustafa, M.I. (2007): Separation flow sheet for high purity concentrates of some Ec. Min. from El-Burullus Baltim sand Dunes Area, North coast, Egypt. The fifth international conference on the geology of Africa, Vol. 1, pp. 111-124.

Moustafa, M. I. (2009): Mineralogical and geochemical studies on monazite – Th, REE silicate series in the Egyptian beach monazite concentrate. Sedimentology of Egypt, Vol. 17, pp. 63-88.

Moustafa, M.I. (2010): Mineralogical characteristics of the separated magnetic rutile of the Egyptian black sands. Resource geology, Vol. 60, Issue, 3, pp. 300-312.

Pettijohn, F. J. (1975): Sedimentary rocks, 3rd Ed., Harper and Row Publ, New York. Robertson

Research International (RRI) Limited (1985): An appraisal of the Rosetta black sands deposit. The Nuclear Materials Corporation, Internal Report, No. 4071, Cairo, Egypt.

Temple, A.K. (1966): Alteration of ilmenite. Econ. Geol., Vol. 61, pp. 695-714.

Wassef, S.N. (1964): Correlation of the sedimentation conditions of the Mediterranean beach east of Damietta to Suez Canal by heavy minerals and isotope applications. M.Sc. Thesis, Fac. Sci., Ain Shams Univ., Egypt.